Journal of
Materials Chemistry B

Materials for biology and medicine

Accepted Manuscript

This article can be cited before page numbers have been issued, to do this please use: Y. Han, Q. Jiang, Y. Li, M. Wang, T. Fan, M. Liu, Q. Ke, H. Xu and Z. Yi, *J. Mater. Chem. B*, 2019, DOI: 10.1039/C9TB01327J.

ROYAL SOCIETY OF CHEMISTRY

rsc.li/materials-b

View Article Online
DOI: 10.1039/C9TB01327J

An aligned porous electrospun fibrous scaffold embedded *Asiatic acid* for accelerating diabetic wound healing

Yiming Han [a,‡], *Yuqi Jiang* [b,‡], *You Li* [a], *Minna Wang* [a], *Tingting Fan* [a], *Mingyao Liu* [a], *Qinfei Ke* [b], *He Xu* [b,*], *Zhengfang Yi* [a, c*]

[a] East China Normal University and Shanghai Fengxian District Central Hospital Joint Center for Translational Medicine, Shanghai Key Laboratory of Regulatory Biology, Institute of Biomedical Sciences and School of Life Sciences, East China Normal University, 200241 Shanghai, China.

[b] College of Chemistry and Materials Sciences, Shanghai Normal University, No. 100 Guilin Road, Shanghai 200234, China

[c] Shanghai Engineering Research Center of Molecular Therapeutics and New Drug Development, School of Chemistry and Molecular Engineering, East China Normal University, Shanghai 200062, China

Yiming Han and Yuqi Jiang are co-first authors.

*Corresponding authors.

E-mail addresses: zfyi@bio.ecnu.edu.cn (Z. Yi), xuhe@shnu.edu.cn (H. Xu)

View Article Online
DOI: 10.1039/C9TB01327J

Abstract

The diabetic non-healing wound is one of the most common complications of diabetics. The long-term stimulus of oxidant-stress, inflammation and infection caused by the hyperglycemia microenvironment in the wound site always leads to the delayed healing process of the diabetic wound. To address this issue, in this study, we prepared an Asiatic acid (AA)-embedded aligned porous poly ($_L$-lactic acid) (PLLA) electrospun fibrous scaffold (AA-PL) for accelerating diabetic wound healing. The results showed that the electrospun fibers with nano-pores on the surfaces aligned in a single direction, while the AA was well embedded in the fibers and can be continuously released from the fibers. The *in vitro* results revealed that the AA-PL scaffolds can effectively alleviate the H_2O_2-induced oxidant-stress damage to HaCat cells and down-regulate the LPS-induced pro-inflammatory cytokines (IL-1β, TNF-α, IL6) gene expression in RAW 264.7 macrophage cells. Moreover, the growth of *E. coli* and *S. aureus* could be inhibited by the AA-PL scaffolds. The *in vivo* study further demonstrated that, the AA-PL scaffolds can accelerate the re-epithelization, angiogenesis and extracellular matrix (ECM) formation of the wound by relieving the high oxidative stress, inflammation and infection in the diabetic wound site. This study suggests that the combination of hierarchical structures (nanopores on the aligned fibers) with the controllable released AA from the scaffolds is an efficient and innovative strategy for the treatment of diabetic non-healing wounds.

Keywords: Electrospun nanofibrous scaffold, aligned porous structure, Asiatic acid, anti-inflammation, diabetic wound healing

View Article Online
DOI: 10.1039/C9TB01327J

1. Introduction

Chronic non-healing wound is one of the most common complications of diabetic patients. As the long-term stimulus of oxidant-stress, inflammation and infection caused by the hyperglycemia microenvironment in the wound site, it leads to the delayed re-epithelialization, insufficient vascular lesions and extracellular matrix （ECM） synthesis of the diabetic wounds. Therefore, it is of great significance to develop an effective strategy to treat diabetic wounds through anti-oxidative stress anti-inflammation or anti-bacteria. [1, 2]

Centella asiatica is a kind of Chinese medicinal herb, and the application of its extraction in wound healing, skin burns, and scar formation had been widely studied. [3, 4] Asiatic acid (AA), has been proven to be the most active substance in the extractions of *Centella asiatica* and it can effectively promote the gene expression of TGF-β (Transforming growth factor-β), VEGF (Vascular endothelial growth factor) and FGFs (Fibroblast Growth Factors) expression in fibroblasts. [5] Most importantly, AA has been demonstrated to have a significant anti-oxidant and anti-inflammatory efficiency in various inflammatory disease models. [6, 7] Beyond that, the anti-bacterial activity of AA has also been verified in many strains. [8] These advantages make AA be a potential drug for treating diabetic wounds. However, an overdose of AA would may have potential side effects such as cytotoxicity and neurotoxicity. [9] Therefore, to develop a controlled-release system with low by-effect is of great importance， which would not only provide sustained and appropriate delivery of AA with an appropriate dose but also increase the utility of AA during the wound healing process. [10, 11]

Electrospinning is one of the most advantageous technique for preparing skin tissue engineering scaffolds. [12] The micro/nano-scaled fibers in electrospun scaffold can not only provide mechanical support for cells adhesion but also promote cell growth with improved bio-guided activity at the wound site by simulating the ECM microenvironment. [13] Normally, the electrospun nanofibers are collected randomly

View Article Online
DOI: 10.1039/C9TB01327J

and the scaffold exhibits a nonwoven structure. In recent years, some researchers have successfully fabricated aligned electrospun scaffolds with the nanofibers arranged in a single direction. Compared with the random nanofibers, the scaffold with aligned nanofibrous structure presents greater potential for skin tissue reconstruction, and the "contact-guided" effect of aligned nanofibers on cells can relatively shorten the time for wound healing. [14, 15] In addition, previous studies have proved that the aligned scaffold could improve the type I collagen expression in the Dural fibroblast cells, and compared with the random scaffolds, the collagen fibers exhibited a higher degree of organization on the aligned scaffolds. [16] Hence, the aligned nanofibrous scaffolds can be a favorable candidate for diabetic wound healing. Moreover, the electrospun fibrous matrices have been widely explored in the biologic delivery systems due to its high drug loading efficiency, so it is an advisable strategy to employ the aligned electrospun scaffolds as a controlled-release system to load AA, and the composite scaffolds will play as a multi-function platform for the effective treatment of diabetic wound.

Meanwhile, it is worth noting that the diabetic non-healing wounds are mainly caused by the failed inflammatory regression in the early stage of wound healing, which ultimately leads to long-term inflammation at the wound sites. Hence, through releasing AA to achieve anti-oxidative stress and anti-inflammatory in the early stage of wound healing will largely improve the therapeutic efficiency of AA. Exactly, the nanofibers with porous surface structure which can not only increase the specific surface area to benefit the cell adhesion, but also can shorten the drug release cycle and promote the AA work in the early stage of diabetic wound healing. [17]

In this study, we developed an aligned porous electrospun fibrous scaffold with a local AA delivery system for accelerating diabetic wound healing. The anti-oxidant stress, anti-inflammation and anti-bacterial effects of aligned porous AA-embedded PLLA electrospun scaffold (AA-PL) *in vitro* were evaluated. Finally, the stimulatory effect of the AA-PL scaffolds on the wound closure, inflammation responses, re-

View Article Online
DOI: 10.1039/C9TB01327J

epithelialization ratio, angiogenesis and ECM remodeling in the STZ-induced diabetes wound model were verified.

2. Materials and methods

2.1 Materials

Poly (L-lactic acid) (PLLA, Mw = 300 kDa) was purchased from Jinan Daigang Biomaterial Co., Ltd. (Shandong, China). Dichloromethane (DCM) was supplied by Aladdin Reagent Co. (Shanghai, China). Asiatic acid (AA) was purchased from Selleck Reagent Co. (Houston, Texas. USA). All materials in this study were used as received without any further purification.

Immortalized human keratinocytes HaCaTs were purchased from the Type Culture Collection of the Chinese Academy of Sciences, Shanghai, China. Mouse mononuclear macrophage cell line RAW 264.7 were purchased from the cell bank, American Type Culture Collection (ATCC, Manassas, VA, USA).

2.2 Preparation of the aligned porous AA-PL scaffolds

The aligned porous fibrous PLLA (PL) scaffold containing different contents of AA (0%, 10%, 30%) were prepared by electrospinning. 0.6 g of PLLA was dissolved in 4.9 mL DCM, and then 0.1 mL AA solution (0 μM, 5 μM, 15 μM in ethanol) was added to the PLLA/DCM solution with continuous stirring to obtain homogeneous solutions. The electrospinning process was carried out using a TEADFS-103 electrospinning apparatus (Beijing Technova Technology Co., Ltd). In a typical procedure, the applied electric voltage was 8 kV, the solution feed rate was 0.02 mL/min, the distance between the spinneret and the grounded drum was 8 cm, the rotating speed of the collecting drum was 800 r/min and the collecting time for all samples was fixed for 3.5 hours.

The experiments were conducted at room temperature, and the relative humidity

View Article Online
DOI: 10.1039/C9TB01327J

was around 50 RH%. All of the as-prepared electrospun scaffolds were vacuum-dried for 24 hours to completely remove the residual solvent prior to further characterization. In this study, the composite electrospun scaffolds with different contents of AA were named as PL, 10 AA-PL and 30 AA-PL, respectively.

2.3 Morphologies, composition and surface wettability characterizations of the aligned porous AA-PL scaffolds

The morphologies and microstructures of the PLLA, 10 AA-PL and 30 AA-PL scaffolds were observed by scanning electron microscopy (FE-SEM, HitachiS-4800, CanScan). The hydrophilicity of electrospun scaffolds were investigated by testing the water contact angle on the surfaces (Kruss GmbH DSA 100 Mk 2).

2.4 AA release profile of the AA-PL scaffolds *in vitro*

0.2 g 10 AA-PL and 30 AA-PL scaffolds were immersed into 5 mL PBS (pH = 7.4) at 37 ℃ in a shaker with the speed of 80 rpm/min, respectively. At each defined time point, 1mL of the release medium was collected for detection and replaced with an equal volume of fresh PBS. The amount of released AA in the collected solution was determined using a UV-vis spectrophotometer (Epoch, BioTek Instruments, Gene Co. Ltd., USA).

2.5 Cell culture

The HaCat and RAW 264.7 were purchased from Sciencell Research Laboratories (San Diego, CA, USA). The HaCat cells were cultured in complete RPMI-1640 cell medium (1640, Gibco, USA) supplemented with 5% fetal bovine serum (FBS, Gibco, USA) and 1% penicillin/streptomycin (P/S, Sciencell, USA). RAW cells were cultured in Dulbecco's Modified Eagle Medium (DMEM, ThermoFisher, USA) supplemented with 5% FBS (Gibco, USA) and 1% P/S (Sciencell, USA). All the cell lines were

View Article Online
DOI: 10.1039/C9TB01327J

cultured in a humidified 37 ℃ / 5% CO_2 incubator and the medium was replaced every 2 days.

2.6 IL-1β, TNF-α and IL6 gene expression level in the LPS-induced inflammation model when co-cultured with AA-PL scaffold

To verified the anti-inflammation effect of AA-PL scaffolds, we stimulated RAW 264.7 macrophage cells with bacterial lipopolysaccharide (LPS) to promote the expression of proinflammatory cytokines, which is the most commonly inflammation model *in vitro*. [19] To detect the expression of proinflammatory cytokine, RAW 264.7 macrophage cells were seeded on the sterile PL, 10 AA-PL, 30 AA-PL nanofibrous scaffolds with a density of 1×10^4 cells /100 μL in 6-well plates. The non-treated (BL) and LPS-treated groups with no scaffold added (Ctrl) were set as the two reference groups. After cultured at 37 °C / 5% CO_2 incubator for 24 hours, the cells of Ctrl, 10 AA-PL and 30 AA-PL treated groups were stimulated with 100 μg/mL of LPS for 6 hours. Finally, the cells were washed with PBS for three times carefully, and then the total RNA of cells were collected with Trizol (Invitrogen, Waltham, MA, USA) according the manufacturer's protocol.

The gene expression of proinflammatory cytokines IL-1β, TNF-α and IL6 was evaluated by quantitative real-time polymerase chain reaction (Q-RT-PCR) according to the manufacturer's protocols. The total RNA (1 μg) was collected and reversed into cDNA by using Prime Script™ RT Master Mix (TakaraBio Inc., Shiga, Japan) at 37 ℃ for 30 min and 85 ℃ for 10 seconds. Subsequently, Q-RT-PCR was conducted by using SYBR Green detection reagent (TakaraBio Inc. Shiga, Japan). In this study, all primers were found in the Primer Bank and synthesized by Genewiz. Co (Shanghai, China), the specificity of the primers was confirmed before being used. The primer sequences used for all PCR reactions were shown in Table 1. β-Actin was used as the housekeeping gene. The expression of each gene was normalized relative to β-Actin and the results

View Article Online
DOI: 10.1039/C9TB01327J

were quantified relative to the corresponding gene expression of the PLLA group, which was standardized to 1.

2.7 Proliferation of HaCat cells treated with high-oxidation stress when co-cultured with AA-PL scaffolds

Before the cell experiments, all scaffolds were cut into round shaped pieces which could exactly fit the size of culture plates, then the scaffolds were sterilized by UV over 3 hours.

HaCat cells were seeded on the PLLA, 10 AA-PL and 30 AA-PL scaffolds with a density of 1×10^4 cells / 200 μL per well in 48-well plates and cultured at 37 °C / 5% CO_2 incubator for 24 hours. To simulate the high oxidative stress environment at the diabetic wound site, HaCat cells in all groups (Ctrl, PL, 10 AA-PL and 30 AA-PL) were treated with 500 μM H_2O_2 for 2 hours, [18] the HaCat cells cultured with no scaffold were considered as control groups (Ctrl). In addition, to verify the high oxidative stress effect of the H_2O_2 on the cell behavior, the non-treated HaCat cells were cultured as the blank groups (BL).

To evaluate the cell viability in different groups, after being cultured for 24 hours, the H_2O_2-treated or non-treated HaCat cells in all four groups were stained with a LIVE/DEAD® Viability Kit (ThermoFisher, USA) according to the supplier's procedure. The cell viability and morphology were observed and photographed using an inverted fluorescence microscope (Leica TCS SP8, Germany), then quantified the number of Live/Dead cell in 10× magnification with Image J, and calculated the ratio of Live/dead cells by the below formation:

Ratio of Live/dead cells = Numbers of live cells/ Total number of cells

To evaluate the cell proliferation in different groups, after incubating the H_2O_2-treated HaCat in 37 ℃ / 5% CO_2 for 2 hours, the cell proliferation was detected by MTS assay. The culture medium was replaced with 160 μL fresh DEME medium and 40 μL

View Article Online
DOI: 10.1039/C9TB01327J

MTS in each well, then the cells were incubated in a 37 ℃ / 5% CO_2 incubator for 1.5 hours. The absorbance value of samples was measured at 490 nm with a microplate reader (Epoch, BIO-TEK, USA).

2.8 Antibacterial effect of the PLLA, 10 AA-PL, 30 AA-PL scaffolds

0.1g sterilized PL, 10 AA-PL, 30 AA-PL scaffolds were soaked in 1 mL LB medium for 48 hours, then 10^8 CFU *E. coli* (ATCC 8739) and *S. aureus* (ATCC 29213) were cultured with the extract solution of PL, 10 AA-PL, 30 AA-PL and 25 ug/mL Penicillin for 24 hours. Then, diluted the bacterial solution to 1×10^6 times and coated 10 μL diluted bacterial solution on the Agar-LB solid medium. After incubated in a 37 °C incubator for 24 hours, the colonies in each group were observed and photographed by high resolution camera (Canon, Japan), then calculated the bacterial concentration of each treated group by Image J.

2.9 Establishment of the non-contractile diabetic wound model

50 males C57BL/6J mice (7-8 weeks age) were purchased from Shanghai Jinlake Experimental Animal Center. The experimental was performed in the specific pathogen free (SPF) environment and all experimental procedures involving mice were given approval by the Animal Investigation Committee of the Institute of Biomedical Sciences and School of Life Sciences, East China Normal University.

The streptozotocin (STZ) (Sigma, USA) - induced diabetic model was established as previously described, [20] STZ was diluted with a citric acid buffer (pH = 4.2-4.5), and the mice were injected intraperitoneally with a dose of 40 mg/kg body weight per day for 5 consecutive days. After 10 days, the blood glucose of the mice was detected with glucose meters device (Accu-Chek Performa) and the mice were considered as diabetics if the non-fasted glycaemia was higher than 20 mM. Mice (n = 12/group) were randomly allocated to the Ctrl, PL, 10 AA-PL and 30 AA-PL treated groups according to the glucose levels.

View Article Online
DOI: 10.1039/C9TB01327J

The diabetic mice (17-18 weeks age) were anesthetized with inhaled 5% isoflurane and shaved the dorsal hair of mice before surgery. A full-thickness circular skin wounds with the diameter of 8 mm were created on the dorsum of each mice and fixed with a silicone loop (silicone sheet, 3M, USA) (internal diameter = 8 mm, external diameter = 15 mm) to prevent contraction of wounds, thus simulating the wound healing process of diabetes. [21] The wounds were treated with different kinds of to-be-tested scaffolds (PL, 10 AA-PL, 30 AA-PL) or non-treated (Ctrl). All the wounds in the four groups were covered with the medical grade bandages (HAINUO, China) and breathable films (Tegaderm, 3M, USA) after surgery. For wound healing assay, the wound areas were photographed on day 0, 3, 5, 7, 11, 13, 15 and calculated by Image J. The wound healing rate was calculated according to the following formula:

$$A_N \text{ rate } (\%) = (A_0 - A_N) / A_0 \times 100\%$$

Where A_0 is the initial wound area (N = 0) and A_N is the wound area at day N ($N \geq 1$).

2.10 Q-RT-PCR, immunohistochemical and immunofluorescence analysis of the wound tissues

About five mice each group were sacrificed at day 7 and day 15 post-surgery, the skin tissue surrounding wound edges with the width of about 2 mm were collected for the Q-RT-PCR, immunohistochemical and immunofluorescence analysis.

The total RNA of re-epithelized skin tissue was extracted by Trizol (Invitrogen, Waltham, MA, USA), the gene expression of proinflammatory cytokine (IL-1β, TNF-α, IL-6) were detected by the method as described above.

For immunohistochemical analysis, the wound tissues were fixed by 4% paraformaldehyde for 48 h. Then, they were dehydrated with a graded series of ethanol (50%, 70%, 80%, 95% and 100%) and embedded in paraffin. The paraffin-embedded tissues were cut into slices with the thickness of 5 μm and tiled on the glass slide.

View Article Online
DOI: 10.1039/C9TB01327J

To evaluate the re-epithelization, collagen deposition, inflammation and angiogenesis in the wound sites of different groups at day 7 and 15 post-operation, the sections were deparaffinized with dimethylbenzene and rehydrated with 100%, 95%, 80% and 70% ethanol. IL6 immunohistochemical staining was performed for the evaluation of inflammation. The Masson trichrome staining was conducted to observe the re-epithelization and collagen deposition. The CD31 (Platelet endothelial cell adhesion molecule-1) immunofluorescence staining was performed to observe the angiogenesis. The Masson trichrome staining were conducted to evaluate the collagen distribution and density, collagen can be stained blue and epithelial or fibroblasts can be dyed red. We evaluated the collagen deposition in the wound tissues by calculated the percentage of collagen fibers area at 20 × magnification with Image J. The formation as below：

Collagen density （%） = Area of collagen fibers / the total area ×100%

All the experimental procedures were conducted according to the supplier's procedure.

Immunohistochemical and immunofluorescence staining was performed just as the follow steps: The samples were boiled in sodium citrate buffer (pH = 6.5) and then incubated with IL6 antibody (Abcam, USA) or CD31 antibody (Abcam, USA) at 4 ℃ for overnight. The sections were incubated with secondary antibodies for 2 hours at room temperature. Adding 5 mg/mL 4', 6-diamidino-2-phenylindole (DAPI) solution to the tissue sections for counterstaining cell nuclei. The images were obtained using an optical microscope (Leica Confocal microscope, Germerny). The collagen area and CD31-positive vessel number were measured manually by Image J software.

2.11 Statistical analysis

Three independent experiments were carried out and at least three samples per each test were taken for statistical analysis. Data were presented means ± standard error.

View Article Online
DOI: 10.1039/C9TB01327J

Statistical differences among more than two groups were calculated using one-way ANOVA firstly and then a Student's t-test program was further conducted to evaluate the significant difference between each two groups. Differences were considered significant when $P< 0.05$(*), $P < 0.01$(**) or $P < 0.001$(***).

3. Results

3.1 Characterization of the aligned porous AA-PL scaffolds

The macroscopic appearance of the AA-PL electrospun scaffolds were shown in Figure S1, the aligned porous AA-PL scaffolds were fabricated with poly (L-lactic acid), so it exhibited as white and smooth membrane, and consisted of the aligned electrospun fibers evenly. The microscopic morphologies of PLLA electrospun scaffolds with different contents of AA were shown in Figure 1, the nanofibers in all the three scaffolds were aligned in a single direction and exhibited well-organized topological structures (Figure 1 A_1-C_1). The magnified SEM images in Figure 1 A_2-C_2 further revealed that there were uniform nanopores on the surface of each fiber in all the three scaffolds.

The hydrophilicity of the PLLA, 10 AA-PL and 30 AA-PL scaffolds were investigated by water contact angle (WAC) measurement. As shown in Figure 1 A_3-C_3, the three scaffolds exhibited a similar surface hydrophilic behavior and the WCA values of the PLLA, 10 AA-PL, 30 AA-PL scaffolds were all about 90°. The hydrophilicity of the scaffolds is improved comparing with pure PLLA polymer, which is more conducive to cell adhesion and growth on the surface of the AA-PL scaffolds. [22]

3.2 The cumulative release of AA from aligned porous AA-PL scaffolds

AA has a remarkable absorbance at 197 nm ultraviolet rays (Figure 2A). As observed in Figure 2B, the UV absorbance curve of the extract solution of PL, 10 AA-PL and 30 AA-PL scaffolds also exhibited a remarkable absorbance at 197 nm, it coincided with the absorbance curve of AA. This result identified that the AA had been successfully incorporated into the aligned porous electrospun scaffolds. As Figure 2B

View Article Online
DOI: 10.1039/C9TB01327J

shown, the cumulative release AA reach to 48 μg from 10 AA-PL and 149 μg from 30 AA-PL, there were approximately 70% of loaded AA released from 10 AA-PL and 30 AA-PL scaffolds (Figure 2C). AA was released rapidly from 10AA-PL and 30 AA-PL scaffolds during the first 48 hours and can be continuously released for 7 days.

3.3 The anti-inflammation and anti-oxidant stress effects of the aligned porous AA-PL scaffolds *in vitro*

Diabetes non-healing wounds are characterized by the long-term inflammation. Here, the common inflammatory model used *in vitro* was constructed by the stimulation of the RAW 264.7 macrophage cells with bacterial lipopolysaccharide (LPS). [23] The expression of pro-inflammatory cytokines in RAW 264.7 macrophage cells were detected by Q-RT-PCR. As shown in Figure 3A-C, the gene expression levels of IL-1β, TNF-αand IL6 in RAW 264.7 macrophage cells were significantly increased after the stimulation by LPS. However, the gene expression levels of above genes in RAW 264.7 macrophage cells were effectively down-regulated in both the 10 AA-PL and 30 AA-PL treated groups, especially for that in the 30 AA-PL group, which showed the lowest gene expression of pro-inflammatory cytokines.

To simulate the high oxidant-stress environment of diabetic wound site, the HaCat cells were treated with 500 μm H_2O_2 after co-cultured with PL, 10 AA-PL, 30 AA-PL scaffolds for 24 hours, then the cells viability were observed by Live/Dead staining and cells proliferation were detected by MTS assay to evaluate the anti-oxidant effect of scaffolds under high oxidative stress. Compared with the non-treated HaCat (BL) shown in Figure 3D(a), after being treated with H_2O_2, there was an obvious shrinkage in cell morphology and quite a lot of dead cells appeared in the view (Figure 3D(b)). Similarly, the H_2O_2-treated HaCat cells co-cultured with the PLLA scaffolds also showed obvious shrinkage morphologies (Figure 3D(c)). However, the H_2O_2-induced oxidant-stress damage of the HaCat cells were effectively alleviated, and the number of viable cells was increased in the AA-PL scaffolds treated groups. Especially for the 30 AA-PL treated group (Figure 3D(e)), the scaffolds significantly improved the

growth and viability of cells. The result (Figure 3E) of proliferation assay showed that, the number of HaCat cells on the 10 AA-PL and 30 AA-PL scaffolds were significantly higher than that of the Ctrl group and PL treated group, indicating the positive effect on the anti-oxidation stress of the 10 AA-PL and 30 AA-PL scaffolds.

3.4 The aligned porous AA-PL scaffolds inhibits *S. aureus* and *E. coil* growth.

The antibacterial property is a crucial factor for an ideal skin tissue engineering scaffold and the high antibacterial activity of scaffold can significantly accelerate the tissue repair process. [24] The minimum inhibitory concentration (MIC) of AA were in the range of 20-40 μg/ml, and its minimum bactericidal concentration (MBC) were in the range of 32-52 μg/ml. The antibacterial effective concentration of AA is comparable to t penicillin, which is the most commonly used antibiotic in clinical. [8] Therefore, the inhibitory effect of Penicillin and AA-PL scaffolds on E. coli (ATCC 8739) and S. aureus (ATCC 29213) were evaluated. As Figure 4 shown, compared with the PLLA treated group, Penicillin (25 μg/mL), 10 AA-PL and 30 AA-PL can significantly inhibit the growth of bacteria, especially 30AA-PL exhibits optimal antibacterial effect. The antibacterial effect of 30 AA-PL is significantly better than that of Penicillin (25 μg/mL), it implied that AA-PL scaffolds may be an alternative strategy for resistant infections of wound in clinically.

3.5 The aligned porous AA-PL scaffolds accelerate diabetic wound healing *in vivo*

The wound healing assay on diabetic mice was performed to further verify the effect of AA-PL scaffolds on the wound healing efficiency *in vivo*. To simulate the low contractility feature of the diabetic wounds in human being, a non-contractile full-thickness diabetic wound model had been constructed in this work and the experimental procedure was shown in Figure 5A. As shown in Figure 5B, the wound area in Ctrl (non-treated), PL, 10 AA-PL and 30 AA-PL groups became smaller with increasing time, while the wound healing rate of the 30 AA-PL scaffolds treated group was

View Article Online
DOI: 10.1039/C9TB01327J

significantly higher than that of the other three groups (Ctrl, PL and 10 AA-PL) from day 3. At day 7 after operation, the healing rates of 30 AA-PL groups was 63.01%, while that of the Ctrl, PL and 10 AA-PL groups were 20.01%, 24.96%, 50.21%, respectively. At the day 14, the wound healing rate of 30 AA-PL group was 97.37%, whereas that of the Ctrl, PL, 10 AA-PL were 50.25%, 66.08%, 94.49% respectively. All above results indicated that the 30 AA-PL scaffolds exhibited the highest wound healing rate among all the treated groups.

3.6 The anti-inflammation effect of the aligned porous AA-PL scaffolds during the diabetic wound healing

Long-term inflammation is an important cause of non-healing diabetic wound. IL6 is a pro-inflammatory cytokine which can be used as a biomarker of inflammation. In this work, the IL6 immunohistochemical staining was performed to evaluate the inflammation level in the wound sites. As observed in Figure 6A, the distribution of IL6-positive cells (brown) were much more densely in the wound tissue of Ctrl, PL and 10 AA-PL treated groups. In contrast, IL-6 positive cells were significantly reduced in the 30 AA-PL treated groups both at day 7 and 15 after surgery. Especially at day 15, the IL 6 positive cells were significantly decreased in the wound tissues of 30 AA-PL treated group and the architecture of normal skin tissue could be obviously observed, suggesting the great anti-inflammatory effect of 30 AA-PL scaffolds during diabetic wound healing. While there were abundant IL 6 positive cells gathered at the wound edges of the Ctrl, PL and 10 AA-PL treated groups. To further verify the anti-inflammation effect of 30 AA-PL scaffolds, the gene expression level of IL-1β, TNF-α and IL6 in wound tissue at day 7（Figure 6 B-D） and day 15 (Figure 6 E-G) were evaluated by Q-RT-PCR. As shown in Figure 6 B-G, the gene expression levels of proinflammatory cytokines: IL1β, TNF-α, and IL6 in the wound tissue of the 30 AA-PL treated groups were obviously the lowest among all treated groups.

3.7 The aligned porous AA-PL scaffolds accelerate re-epithelialization of diabetic wound

Re-epithelialization is a crucial stage in the process of diabetic wound healing, in which stage epithelial keratinocytes will proliferate and migrate from the wound edge to the center of wound tissues, forming a complete epithelial layer. [25]As shown in Figure 7A, the newly formed epithelium layers in 30 AA-PL treated groups were significantly increased than that of the Ctrl, PL, 10 AA-PL treated groups at day 7, and the wound tissue in 30 AA-PL treated group formed much more continuously intact epithelial layer at day 15, indicating a better promoting efficiency on re-epithelialization of 30 AA-PL scaffolds than that of the Ctrl, PL and 10 AA-PL scaffolds. The quantitative analysis results of re-epithelialization were shown in Figure 7B-C revealed that, the re-epithelialization ratio of 30 AA-PL treated groups (64.22%) was significantly higher than that of the Ctrl (8.54%), PL (34.17%), and 10 AA-PL (58.25%) treated groups at day 7. At day 15 after surgery, the re-epithelialization ratio of 30 AA-PL treated group was 94.71%, while that of the Ctrl, PL, 10 AA-PL treated groups were 51.13%, 64.41%, 77.65%, respectively.

3.8 The effect of the aligned porous AA-PL scaffolds on the angiogenesis in the diabetic wound *in vivo*.

The early 3-7 day of wound healing is an important stage for formatting granulation tissue which consisted of fibroblasts and neovascular. In order to verify the angiogenesis during the diabetic wound healing process, the CD31 immunofluorescence staining was performed to observe the neovascularization in the wound tissue at 7 days after surgery. As shown in Figure 8A and B, the number of CD31 positive vessels in the wound tissues of the 10 AA-PL and 30 AA-PL treated groups were obviously higher than that of the Ctrl and PL treated group at day 7. The above results showed that the 10 AA-PL and 30 AA-PL scaffolds promoted angiogenesis during diabetes wound healing.

View Article Online
DOI: 10.1039/C9TB01327J

3.9 The effect of the aligned porous AA-PL scaffolds on ECM formation *in vivo*

As shown in Figure 9A, compared with the Ctrl group, more collagen fibers (ECM remodeling marker, stained with blue) were observed in the PLLA, 10 AA-PL and 30 AA-PL treated groups. Especially, the collagen fibers in the wound tissues of 30 AA-PL treated group were more interweaved and tended to form more intensive and orderly structures at day 15 after surgery. The quantitative analysis of the deposited collagen in the wound sites shown in Figure 9B demonstrated that the collagen deposition in 30 AA-PL treated group (95.97%) was significantly higher than that in the Ctrl (62.15%), PL (75.94%) and 10 AA-PL (88.59%) treated groups. It implied a more advanced collagen deposition process in the 30 AA-PL treated groups.

4. Discussion

Previous studies have mainly focused on improving angiogenesis or antibacterial, as a single strategy for the treatment of diabetic non-healing wounds. [24-27] However, due to the complex pathological environment at the diabetic wound site, those efficiencies are limited. Since the most essential causes of the diabetic non-healing wounds are hyper oxidative stress, inflammation and infection, which were caused by the hyperglycemia microenvironment in wound sites, [28, 29] alleviating the oxidant-stress, inflammation and infection at the wound site will be an effective strategy for diabetic wound healing. [30] AA was proved to be a potential drug for diabetes by the antioxidant, anti-inflammatory and antibacterial efficiencies. In this study, AA was chosen as an active ingredient incorporated into an aligned porous composite P_LLA scaffolds via electrospinning for highly efficient diabetic wound healing.

Since the aligned nanofibers have been proven to have significant impacts on directing the cellular alignment and migration by “contact guidance”, which could accelerate cells migrate from the edge to the center of wound, so the aligned nanofibers have advantage on preparing wound dressing. [31] What’s more, the porous surface of aligned nanofibers not only could enhance the surface roughness, which benefit for cell adhesion and proliferation; but also increase the effective surface area of membranes,

which conducive to drug loading and release continuously. Herein, we successfully fabricated an aligned PLLA electrospun scaffold as the drug-dlivery system, Figure 1 showed that the PLLA fibers in electrospun scaffolds were orderly aligned in a single direction, as a result of the combined effects of the electrostatic force in the electric field and the stretching force of the collecting drum during the electrospinning process.

Diabetic wound is characterized of the oxidant stress, prolonged inflammatory and infection caused by the hyperglycemia microenvironment, which will prevent the diabetic wound at prolonged inflammation phase transfer to the next proliferation phase. Hyperglycemia and extra-oxidative stress environment of wound sites impaired macrophage and neutrophils function result in the prolonged inflammation; the impaired keratinocyte cause delay re-epithelialization; impaired fibroblast and vascular endothelial cells lead the insufficient granulation tissue and ischemia. The hyperglycemia environment also makes the wound tissues more susceptible to be infected, further cause the chronic non-healing wound. Overall, the hyperglycemia and oxidative stress are the root causes of diabetic non-healing wounds. [32, 33]

In this study, to relieve those symptoms the early stage of wound healing and promote the transition of wound from inflammation to the proliferation phase, we have chosen *Asiatic acid* (AA), a Chinese herbal compound, which have the anti-oxidant, anti-inflammation and anti-bacteria effect, as a potential drug for diabetic wounds. The uniform nanopores with ellipse-like morphologies were generated on the surface of each fiber by using low boiling solvent during the electrospinning process, and these nanopores on the surfaces of fibers could facilitate the release of AA at the early stage of diabetes wound healing. As illustrated in Figure 2, AA was well embedded in the fibers and can be continuously released from 10 AA-PL and 30 AA-PL for 7 days, which could exactly meet the requirement of the early inflammation stage (3-7 days after trauma) during the diabetic wound healing. [34]

Macrophages is the foremost producer of pro-inflammatory cytokines IL-1β, TNF-α, IL-6 and VEGF, IGF-1 and TGF-β, they are pivotal contributor both in diabetic and non-healing wound healing. [35-37] Usually, those cytokines and growth factors are increased in the early 3 days and decreased gradually after inflammation phase. While

in diabetes wound, pro-inflammatory cytokines sustain production continuously, caused the prolonged inflammation phase, it leads the extra-oxidant stress environment on the wound site, further impaired the angiogenic response, migration and proliferation of keratinocytes and fibroblast. [38, 39] Therefore, eliminating inflammation, it can effectively regulate the levels of cytokines and growth factors during wound healing. It has been reported that the expression of pro-inflammatory factors of macrophages is elevated when exposing in LPS stimuli, it usually triggered by activation of NF-KB. While AA may down-regulate NF-κB (nuclear factor-κB) activation in RAW 264.7 MACROPHAGE cells,[39] and further reduce proinflammation cytokines IL-1β, TNF-α and IL6 production to attenuated the prolonged inflammation. In this work, the 10 AA-PL and 30 AA-PL scaffolds have significantly down-regulated the high expression of pro-inflammatory cytokinesIL-1β, TNF-α, IL6 (Figure 3A-C) in LPS-induced macrophage inflammation model *in vitro*. In STZ-induced diabetes non-contraction wound model, with the increasing content of AA, the IL-6 expression in the diabetes wound sites had been reduced in the 10 AA-PL and 30 AA-PL treated groups.

The prolonged inflammation could cause high oxidative stress microenvironment at wound sites, it especially induces the injury, dysfunction, and apoptosis of keratinocyte, further result in the delayed re-epithelialization. [29, 40] H_2O_2 could inducing excessive ROS (Reactive oxygen species) in cells, damage cell membranes and mitochondria, further leading cell apoptosis, so we treated the HaCat cells with H_2O_2 to simulate the supra-physiological oxidative stress microenvironment in diabetic wound sites *in vitro*. Previous study has proven that AA could prevent oxidative stress and apoptosis by maintaining membrane integrity and ATP production. [41] Therefore, we evaluated the protect effect of AA-PL scaffolds on HaCat under oxidative stress, As Figure 3D-E showed, the AA-PL exhibited significant protect effect on morphology and proliferation of HaCat cells which damaged by H_2O_2 induced supra-oxidant stress *in vitro* and accelerated re-epithelialization during diabetes wound healing (Figure 7) *in vivo*.

Infection caused by hyperglycemia microenvironment in the wound sites was another main barrier for diabetes wound healing. Previous studies have proved that AA

View Article Online
DOI: 10.1039/C9TB01327J

could destroy the biofilm of the bacterial community and the cell membrane of individual cells, which cause bacterial nuclear leakage to achieve antibacterial purposes dose-dependently. [42-44] Consistent with previous researches, 30 AA-PL scaffolds also exhibited the best anti-bacterial effect among all treated groups (Figure 4).

Sum up the above results, we can ensure that the AA-PL scaffolds could release effective concentration of AA in the safe range, and exhibited great effect on anti-oxidative stress, anti-inflammation and anti-bacteria *in vitro*. To further verify the effect of AA-PL scaffolds on accelerating diabetes wound *in vivo*, and exploring that whether the aligned porous structure and released AA could improve non-healing wounds synergistically, the wound healing assay was performed in the STZ-induced diabetes non-contraction wound model. In accordance with the significant effect of AA-PL scaffolds *in vitro*, the diabetic wounds treated with AA-PL scaffolds showed higher wound healing rate as compared with that of the PLLA and Ctrl groups starting from the day 3 after surgery, especially for that of the 30 AA-PL scaffolds, which exhibited the highest wound healing rate (Figure 5) by down-regulating IL-1β, TNF-α, IL6 gene expression (Figure S2 and 6) and accelerating re-epithelialization (Figure 7), angiogenesis (Figure 8) and collagen deposition (Figure 9) in diabetes wound site. The underlying mechanism may relate to the anti-oxidative stress, anti-inflammation and antibacterial effect of AA-PL, which are conducive to alleviate those symptoms of diabetes non-healing wound, further promoting the non-healing wound at long-term inflammation phase transferred into the proliferation phase during diabetes wound healing. [45, 46] The overall microenvironmental change at the wound sites induced by AA-PL scaffold promoted faster healing process for diabetic wounds. What's more, consistent with the previous study, the aligned PL scaffolds can shorten the time of wound healing by facilitating the migration of keratinocytes and fibroblasts from the periphery of the wound to the center, and significantly promote re-epithelization and collagen formation during the process of wound healing. [47, 48] Hence, in this work, the aligned porous structure of AA-PL indeed provided bio-guidance and mechanical support to facilitate diabetes wound healing. In conclusion, AA-PL scaffolds provided a suitable environment for wound healing through the dual advantages of AA release

and aligned porous structure, which can be used as an excellent scaffold for promoting diabetic wound healing.

5. Conclusion

In this study, an Asiatic acid (AA)-embedded aligned porous poly ($_L$-lactic acid) (PLLA) electrospun fibrous scaffold had been successfully fabricated for accelerating diabetic wound healing. AA was embedded in aligned porous electrospun fibrous scaffolds, and could sustain release from the AA-PL scaffolds. Especially, the 30 AA-PL scaffolds could effectively alleviate the oxidant-stress damage to HaCat cells and down-regulate gene expression of pro-inflammatory cytokines, as well as anti-bacteria *in vitro*. The *in vivo* study further evidenced that 30 AA-PL exhibited an excellent effect on accelerating re-epithelization, angiogenesis and ECM formation during diabetes wound healing in diabetic mice. Above results suggest that the combination of hierarchical aligned structures with the controllable released AA from the scaffolds is an efficient and innovative strategy for the treatment of diabetic non-healing wounds and other types of skin injure.

Acknowledgments

This study was partially supported by National Natural Science Foundation of China (81472788, 81773204, 81330049, 81501597), National Key R&D Program of China (2018YFA0507000), Major State Basic Research Development Program of China (2015CB910400), and Innovation Program of Shanghai Municipal Education Commission (2017-01-07-00-05-E00011).

Author contribution

Yiming Han and Yuqi Jiang contributed equally to this work. Yiming Han, Yuqi Jiang, He Xu and Zhengfang Yi designated the idea of the present work. He Xu, Qinfei Ke, Mingyao Liu and Zhengfang Yi supervised the project and commented on the project. Yuqi Jiang and He Xu synthesized and characterized the AA-PL scaffolds, Yiming Han

performed *in vitro* experiments and *in vivo* experiments, analyzed the dates. You Li contributed to the anti-bacteria assay. Minna Wang and Tingting Fan were assist in completing diabetes wound healing experiments. Yiming Han wrote the manuscript. All the authors contributed to the discussion during the whole project.

Reference

[1] S.A. Eming, P. Martin, M. Tomic-Canic 2014 Wound repair and regeneration: Mechanisms, signaling, and translation, *Sci. Transl. Med.* **6** 1946-6242

[2] C.C. Lan, C.S. Wu, S.M. Huang, I.H. Wu, G.S. Chen 2013 High-glucose environment enhanced oxidative stress and increased interleukin-8 secretion from keratinocytes: new insights into impaired diabetic wound healing, *Diabetes.* **62** 2530-2538

[3] W. Bylka, P. Znajdek-Awizen, E. Studzinska-Sroka, A. Danczak-Pazdrowska, M. Brzezinska 2014 Centella asiatica in dermatology: an overview, *Phytother. Res.* **28** 1117-1124

[4] Veeraya Paocharoen MD 2010 The efficacy and side effects of Oral Centella asiatica extract for wound healing promotion in diabetic wound patients. *J Med Assoc Thai*. **93** s166-s170

[5] Christopher D and Puziah Hashim 2003 Gene expression Changes in the human fibroblast induced by Centella asiatica Triterpenoids, *Planta Med.* **69** 725-732

[6] J.W. Lv, A. Sharma, T. Zhang, Y.C. Wu, X.T. Ding 2018 Pharmacological Review on Asiatic Acid and Its Derivatives: A Potential Compound, *Slas Technology.* **23** 111-127

[7] Y.S. Qian, Z.C. Xin, Y.N. Lv, Z.W. Wang, L. Zuo, X. Huang, Y.M. Li, H.B. Xin 2018 Asiatic acid suppresses neuroinflammation in BV2 microglia via modulation of the Sirt1/NF-kappa B signaling pathway, *Food Funct.* **9** 1048-1057

[8] W.H. Liu, T.C. Liu, M.C. Mong 2015 Antibacterial effects and action modes of asiatic acid, *Biomedicine (Taipei)*. **5** 16

[9] Y.Q. Meng, H.B. Cui, L. Li, W.C. Zhang, H.S. Pan, T.T. Yu, W. Li 2018 Synthesis and antitumor activity evaluation of asiatic acid derivatives as survivin inhibitor, *J*

View Article Online
DOI: 10.1039/C9TB01327J

Asian Nat Prod Res. **20** 1-12

[10] J.S. Choi, H.S. Kim, H.S. Yoo 2015 Electrospinning strategies of drug-incorporated nanofibrous mats for wound recovery, *Drug Delivery and Translational Research.* **5** 137-145

[11] W. Cui, Y. Zhou, J. Chang 2010 Electrospun nanofibrous materials for tissue engineering and drug delivery, *Sci Technol Adv Mater.* **11** 14-108

[12] N. Bhardwaj, S.C. Kundu 2010 Electrospinning: a fascinating fiber fabrication technique, *Biotechnol Adv.* **28** 325-347

[13] H. Chen, Y. Peng, S. Wu, L.P. Tan 2016 Electrospun 3D Fibrous Scaffolds for Chronic Wound Repair, *Materials (Basel).* **9** 272-284

[14] H.N. Kim, Y. Hong, M.S. Kim, S.M. Kim, K.Y. Suh 2012 Effect of orientation and density of nanotopography in dermal wound healing, *Biomaterials.* **33** 8782-8792

[15] H. Xu, F. Lv, Y. Zhang, Z. Yi, Q. Ke, C. Wu, M. Liu, J. Chang 2015 Hierarchically micro-patterned nanofibrous scaffolds with a nanosized bio-glass surface for accelerating wound healing, *Nanoscale.* **7** 18446-18452

[16] J.W. Xie, M.R. MacEwan, W.Z. Ray, W.Y. Liu, D.Y. Siewe, Y.N. Xia 2010 Radially Aligned, Electrospun Nanofibers as Dural Substitutes for Wound Closure and Tissue Regeneration Applications, *Acs Nano*. **4** 5027-5036

[17] S.F. Chou, D. Carson, K.A. Woodrow 2015 Current strategies for sustaining drug release from electrospun nanofibers, *Journal of Controlled Release*. **220** 584-591

[18] Y. Xiao, L.A. Reis, N. Feric, E.J. Knee 2016 Diabetic wound regeneration using peptide-modified hydrogels to target re-epithelialization, *P Natl Acad Sci USA.* **113** E5792-E5801

[19] Y.K. Choi, B.R. Ye, E.A. Kim, J. Kim 2018 Bis (3-bromo-4,5-dihydroxybenzyl) ether, a novel bromophenol from the marine red alga Polysiphonia morrowii that suppresses LPS-induced inflammatory response by inhibiting ROS-mediated ERK signaling pathway in RAW 264.7 macrophages, *Biomed Pharmacother.* **103** 1170-1177

[20] Rachel D. Wilson, Md. Shahidul Islam 2012 Fructose-fed streptozotocin-injected rat: an alternative model for type 2 diabetes. Phamacological Reports. **64** 129-139

[21] X.S. Wang, J.F. Ge, E.E. Tredget, Y.J. Wu 2013 The mouse excisional wound

splinting model, including applications for stem cell transplantation, *Nat. Protoc.* **8** 302-309

[22] G. Birhanu, H. Akbari Javar, E. Seyedjafari, A. Zandi-Karimi, M. Dusti Telgerd, 2018 An improved surface for enhanced stem cell proliferation and osteogenic differentiation using electrospun composite PLLA/P123 scaffold, *Artif Cells Nanomed Biotechnol.* **46** 1274-1281

[23] Z.L. Zhai, S.E. Gomez-Mejiba, D.C. Ramirez 2013 The Nitrone Spin Trap 5,5-Dimethyl-1-pyrroline N-oxide Affects Stress Response and Fate of Lipopolysaccharide-Primed RAW 264.7 Macrophage Cells, *Inflammation*. **36** 346-354

[24] Andrews KL, Houdek MT, Kiemele LJ 2015 Wound management of chronic diabetic foot ulcers: from the basics to regenerative medicine. *Prosthet Orthot Int*. Feb **39** 29-39

[25] H.N. Huang, C.Y. Pan, H.Y. Wu, J.Y. Chen 2017 Antimicrobial peptide Epinecidin-1 promotes complete skin regeneration of methicillin-resistant Staphylococcus aureus infected burn wounds in a swine model, Oncotarget. **8** 21067-21080

[26] Uzoagu A. Okonkwo and Luisa A. DiPietro 2017 Diabetes and Wound Angiogenesis, *Int. J. Mol. Sci*.**18** 1419-1434

[27] C.L. Rettinger, J.L. Fletcher, A.H. Carlsson, R.K. Chan 2017 Accelerated epithelialization and improved wound healing metrics in porcine full-thickness wounds transplanted with full-thickness skin micrografts, *Wound Repair and Regeneration.* **25** 816-827

[28] S. Hazarika, A.O. Dokun, Y. Li, A.S. Popel 2007 Impaired angiogenesis after Hindlimb ischemia in type 2 diabetes Mellitus - Differential regulation of vascular endothelial growth factor receptor 1 and soluble vascular endothelial growth factor receptor 1, *Circulation Research.* **101** 948-956

[29] X.M. Chen, J.C. Qian, L.T. Wang 2018 Kaempferol attenuates hyperglycemia-induced cardiac injuries by inhibiting inflammatory responses and oxidative stress, *Endocrine.* **60** 83-94

[30] C.C.E. Lan, C.S. Wu, S.M. Huang, I.H. Wu, G.S. Chen 2013 High-Glucose

Environment Enhanced Oxidative Stress and Increased Interleukin-8 Secretion From Keratinocytes New Insights Into Impaired Diabetic Wound Healing, *Diabetes.* **62** 2530-2538

[31] T. Mustoe 2004 Understanding chronic wounds: a unifying hypothesis on their pathogenesis and implications for therapy, *Am. J. Surg.* **187** 65-70

[32] L. Zhang, L. Xu, G. Li, Y. Yang 2018 Fabrication of high-strength mecobalamin loaded aligned silk fibroin scaffolds for guiding neuronal orientation, *Colloids Surf B Biointerfaces.* **173** 689-697

[33] Satish Patel, Shikha Srivastava 2019 Mechanistic insight into diabetic wounds: Pathogenesis, molecular targets and treatments trategies to pace wound healing. *Biomedicine & Pharmacotherapy* **112** 108615-30

[34] K. Kaltalioglu, S. Coskun-Cevher 2015 A bioactive molecule in a complex wound healing process: platelet-derived growth factor, *Int J Dermatol.* **54** 972-977

[35] R.B. Mateo, J.S. Reichner, J.E. Albina 1994 Interleukin-6 Activity in Wounds, *Am J Physiol.* **266** 1840-1844

[36] T.J. Fahey, A. Sadaty, W.G. Jones 1991 Diabetes impairs the late inflammatory response to wound healing, *J Surg Res.* **50** 308-313

[37] R.E. Mirza, M.M. Fang, W.J. Ennis, T.J. Koh 2013 Blocking Interleukin-1 beta Induces a Healing-Associated Wound Macrophage Phenotype and Improves Healing in Type 2 Diabetes, *Diabetes.* **62** 2579-2587

[38] H.M. Lv, Z.M. Qi, S.S. Wang 2017 Asiatic Acid Exhibits Anti-inflammatory and Antioxidant Activities aganist Lipopolysaccharide and D-Galactosamine-Induced Fulminant Hepatic Failure, *Front Immunol.* **8** 785-801

[39] K.J. Yun, J.Y. Kim, J.B. Kim, K.W. Lee, S.Y. Jeong 2008 Inhibition of LPS-induced NO and PGE(2) production by asiatic acid via NF-kappa B inactivation in RAW 264.7 macrophages: Possible involvement of the IKK and MAPK pathways, *Int Immunopharmacol.* **8** 431-441

[40] Q. Li, I.M. Verma 2002 NF-kappaB regulation in the immune system, *Nat Rev Immunol.* **2** 725-734

[41] H.Q. Ding, Y.Y. Xiong, J. Sun, C. Chen, J. Gao, H.X. Xu 2018 Asiatic Acid

Prevents Oxidative Stress and Apoptosis by Inhibiting the Translocation of alpha-Synuclein Into Mitochondria, *Front Neurosci-Switz.* **12** 431-441

[42] D. Wojnicz, D. Tichaczek-Goska, K. Korzekwa, M. Kicia, A. Hendrich 2017 Anti-enterococcal activities of pentacyclic triterpenes, *Advances in Clinical and Experimental Medicine.* **26** 483-490

[43] W.H. Liu, T.C. Liu, M.C. Mong 2015 Antibacterial effects and action modes of asiatic acid, *Biomedicine-Taiwan*. **5** 22-29

[44] B. Nie, H. Ao, J. Zhou, T. Tang, B. Yue 2016 Biofunctionalization of titanium with bacitracin immobilization shows potential for anti-bacteria, osteogenesis and reduction of macrophage inflammation, *Colloids Surf B Biointerfaces.* **145** 728-739

[45] H.B. Yang, K.T. Nguyen, D.T. Leong, N.S. Tan, C.Y. Tay 2016 Soft Material Approach to Induce Oxidative Stress in Mesenchymal Stem Cells for Functional Tissue Repair, *ACS Appl. Mater. Interfaces.* **8** 26591-26599

[46] R. Costa, R. Negrao, I. Valente, A. Castela, D. Duarte, L. Guardao, P.J. Magalhaes, J.A. Rodrigues, J.T. Guimaraes, P. Gomes, R. Soares 2013 Xanthohumol Modulates Inflammation, Oxidative Stress, and Angiogenesis in Type 1 Diabetic Rat Skin Wound Healing, *J Nat Prod.* **76** 2047-2053

[47] K. Kaltalioglu, S. Coskun-Cevher 2015 A bioactive molecule in a complex wound healing process: platelet-derived growth factor, *Int. J. Dermatol.* **54** 972-977

[48] H.N. Hasmad, M.R. Yusof, Z.R. Mohd Razi, R.B. Haji Idrus, S.R. Chowdhury 2018 Human amniotic membrane with aligned electrospun fiber as scaffold for aligned tissue regeneration, *Tissue Eng Part C Methods.* **24** 368-378

View Article Online
DOI: 10.1039/C9TB01327J

Figure

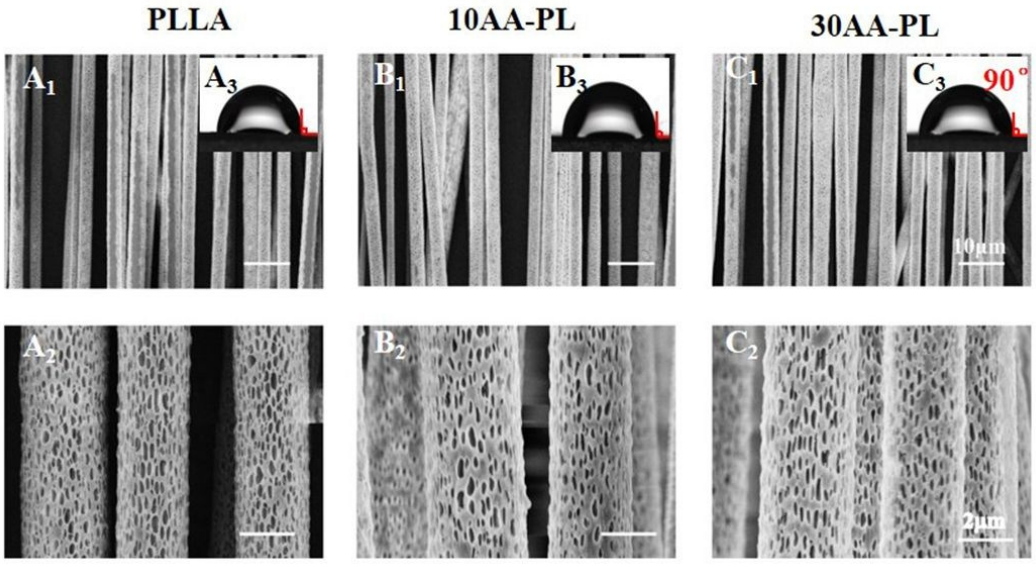

Figure 1. SEM images of the aligned porous PLLA (A_1, A_2), 10 AA-PL (B_1, B_2), 30 AA-PL (C_1, C_2) scaffolds; The insert of each panel in Figure A_3-C_3 showed the water droplet sat on the surface of each scaffold.

View Article Online
DOI: 10.1039/C9TB01327J

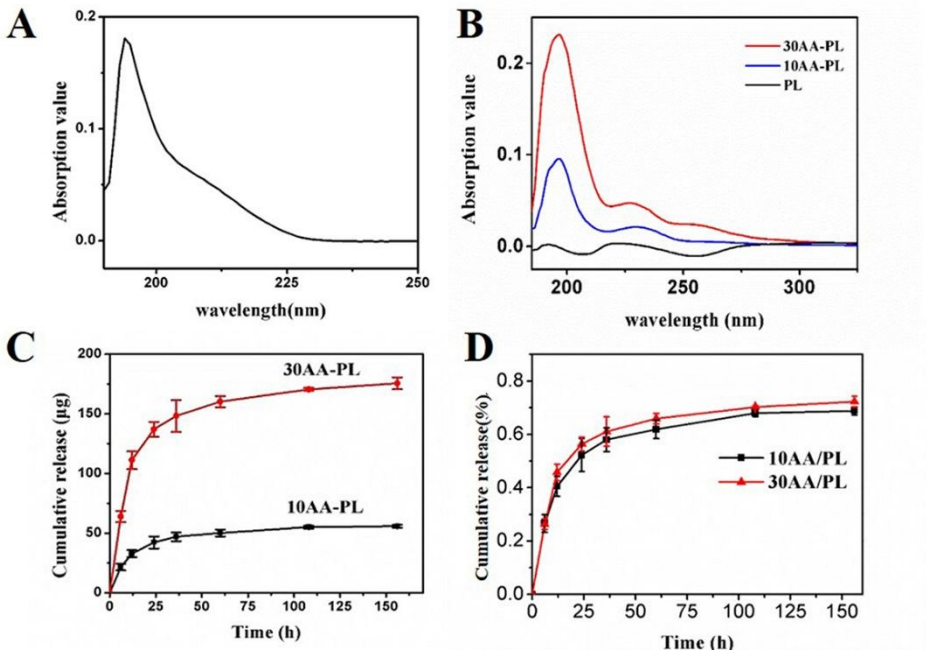

Figure 2. (A) The ultraviolet (UV) ray's absorbance curve of AA; (B) The extract solution of PLLA, 10 AA-PL and 30 AA-PL scaffolds. (C)The cumulative release amount and (D) cumulative release percentage of AA released from 10 AA-PL and 30 AA-PL scaffolds within 7 days.

View Article Online
DOI: 10.1039/C9TB01327J

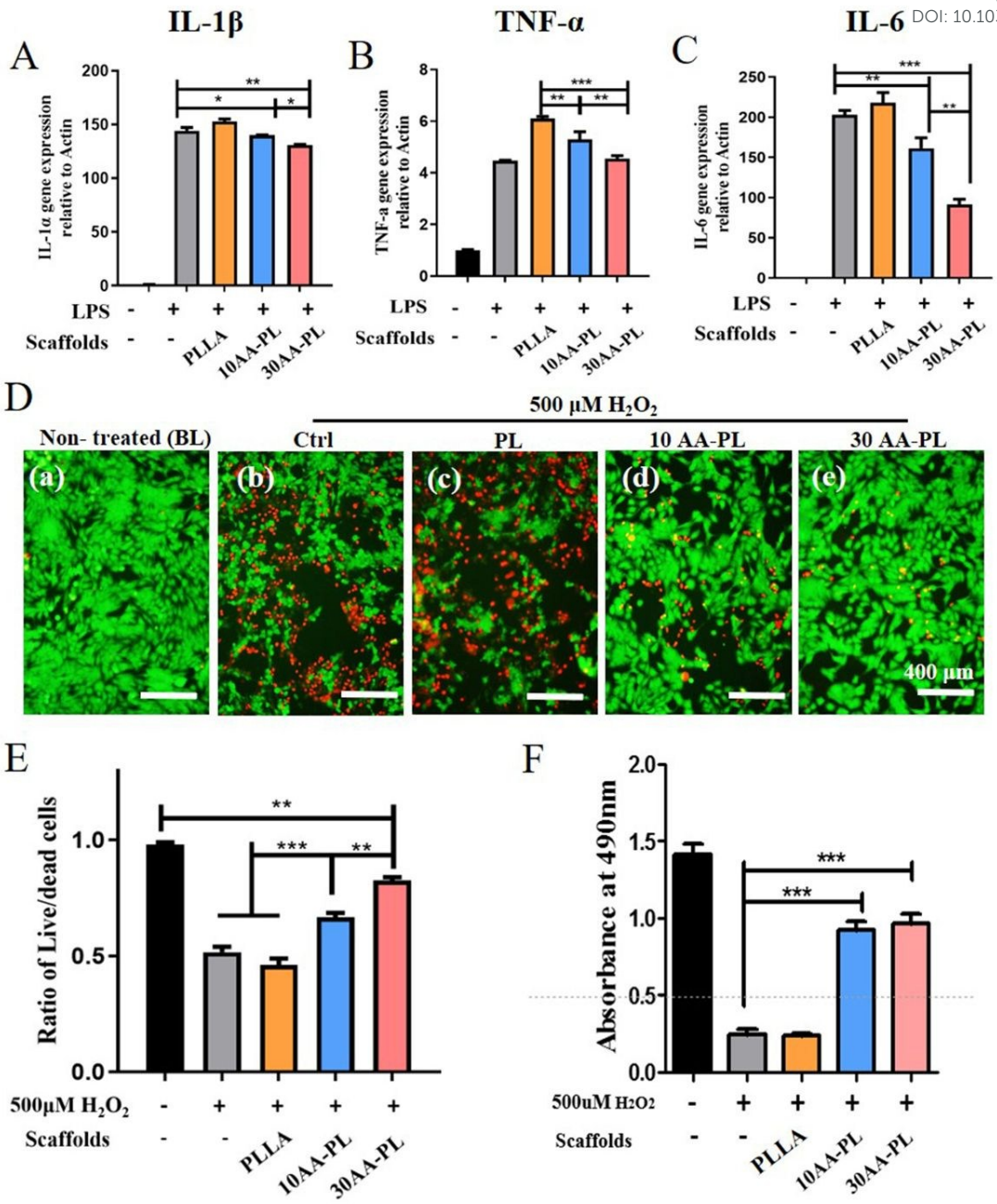

Figure 3. The gene expression levels of proinflammatory cytokines: IL-1β(A), TNF-α(B) and IL6(C) in LPS-induced inflammatory RAW 264.7 macrophage cells while the RAW 264.7 cells were co-cultured with PL, 10 AA-PL and 30 AA-PL (D) Live/Dead staining was performed to detect the cell viability of HaCat cells cultured with different treatments: (a) non-treated (BL); (b) only treated with 500 μM H_2O_2 (Ctrl); (c-e) HaCat cells cultured on the PLLA (c), 10 AA-PL(d), 30 AA-PL (e) scaffolds and stimulated by 500 μM H_2O_2 for 2 hours (scale bar = 400 μm), respectively. (E) Quantified the ratio of Live/dead cells (F)The corresponding cell proliferation of HaCat cells cultured with

different treatments as described in Figure 3D. (* P < 0.05; **P < 0.01; *** P < 0.001)

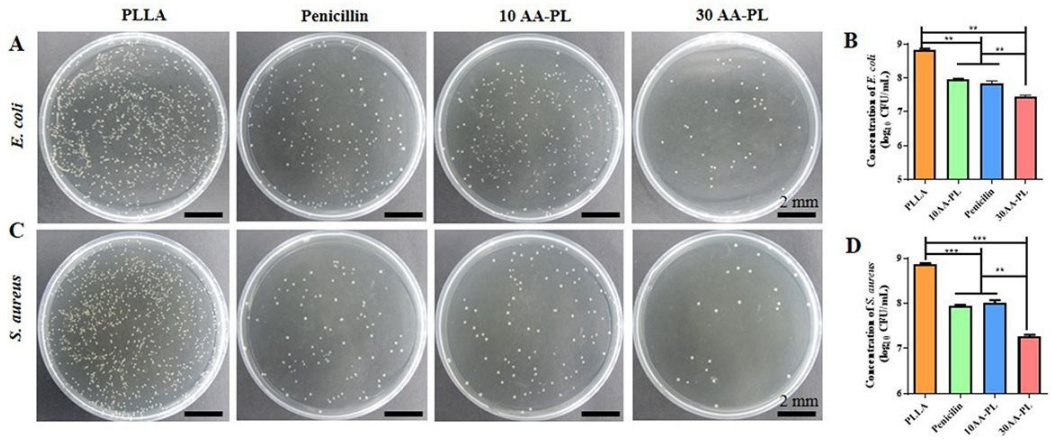

Figure 4. *E. coli* (A) and *S. aureus* (C) were co-cultured with the PLLA, Penicillin (25 ug/mL), 10 AA-PL, 30 AA-PL scaffolds, then diluted to 10^6 and coated the bacterial solution on agar-containing LB solid medium (scale bar = 2 mm); The corresponding statistics of the total number of the *E. coli* (B) and *S. aureus* (D) colonies in the different treated groups. (* P < 0.05 ; **P < 0.01 ; *** P < 0.001)

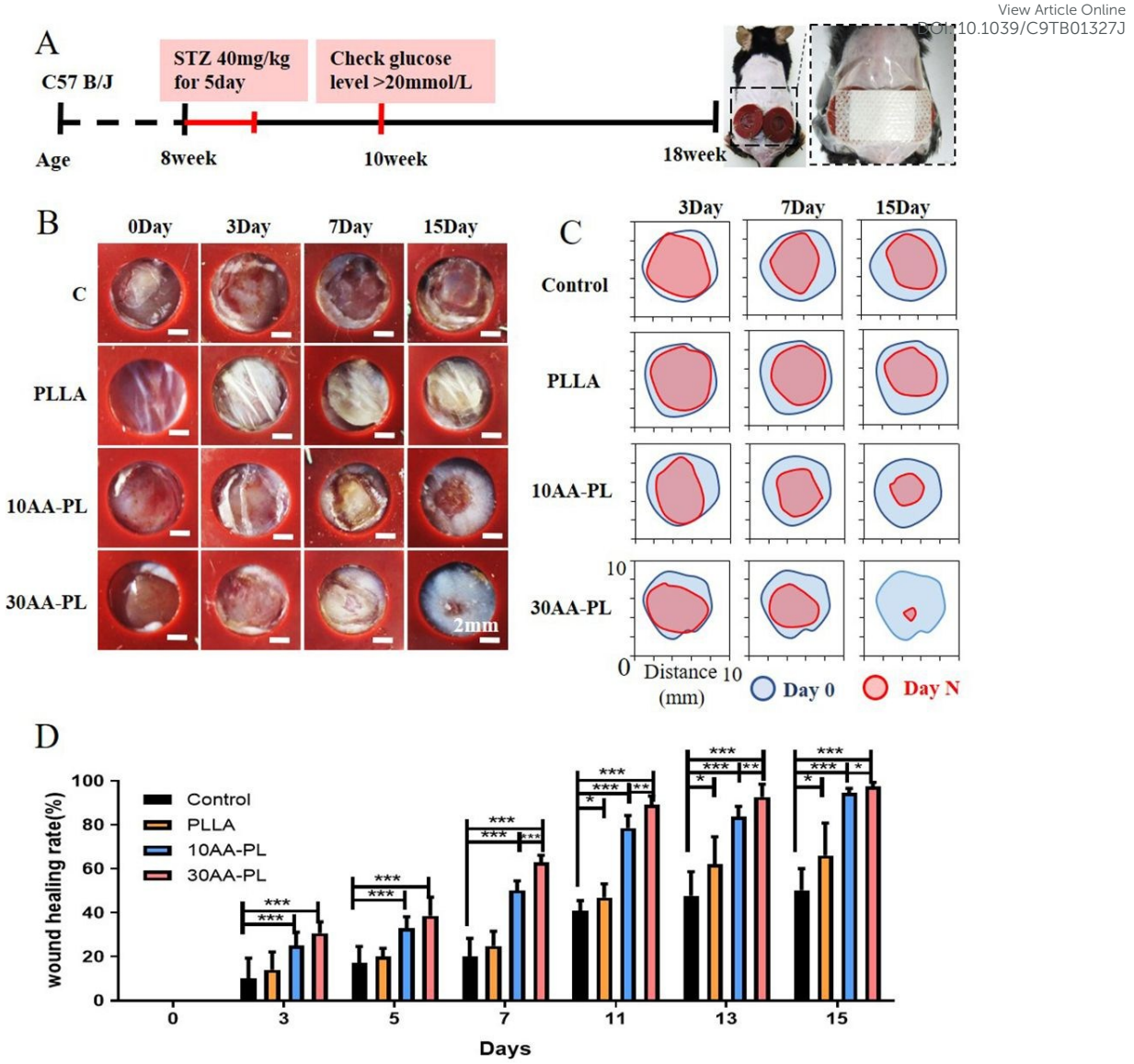

Figure 5. (A) Schematic diagram of the establishment of the non-contractile diabetic wound model ; (B) Overview of the size change of the wounds in different groups (Ctrl, PLLA, 10 AA-PL, 30 AA-PL) on day 0, 3, 7 and 15 after surgery (scale bar = 2 mm); (C) Wound trace for each treatment group on day N (red area represented the wound area at day N, N = 3, 7 and 15) after surgery relative to day 0 (blue area represented the wound area at day 0) *in vivo*. (D) Statistics analysis of the wound healing rate of PL, 10 AA-PL, 30 AA-PL treated groups on day 0, 3, 5, 7, 11, 13, 15 after surgery. (* $P < 0.05$; **$P < 0.01$; *** $P < 0.001$)

View Article Online
DOI: 10.1039/C9TB01327J

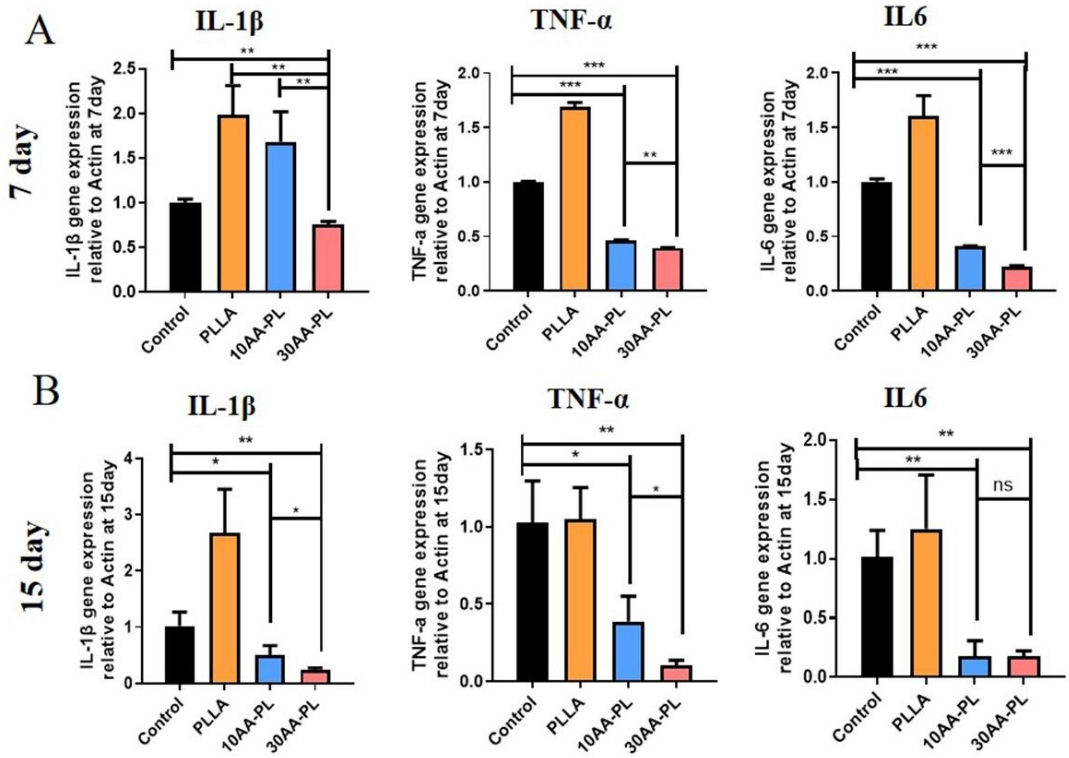

Figure 6. (A) The gene expression levels of IL-1β (B), IL6 and TNF-α in the wound tissues of different groups at day 7 after operation, respectively. (B) The gene expression levels of IL-1β, TNF-α and IL6 in the wound tissues of different groups at day 15 after operation, respectively. (* $P < 0.05$; **$P < 0.01$; *** $P < 0.001$)

View Article Online
DOI: 10.1039/C9TB01327J

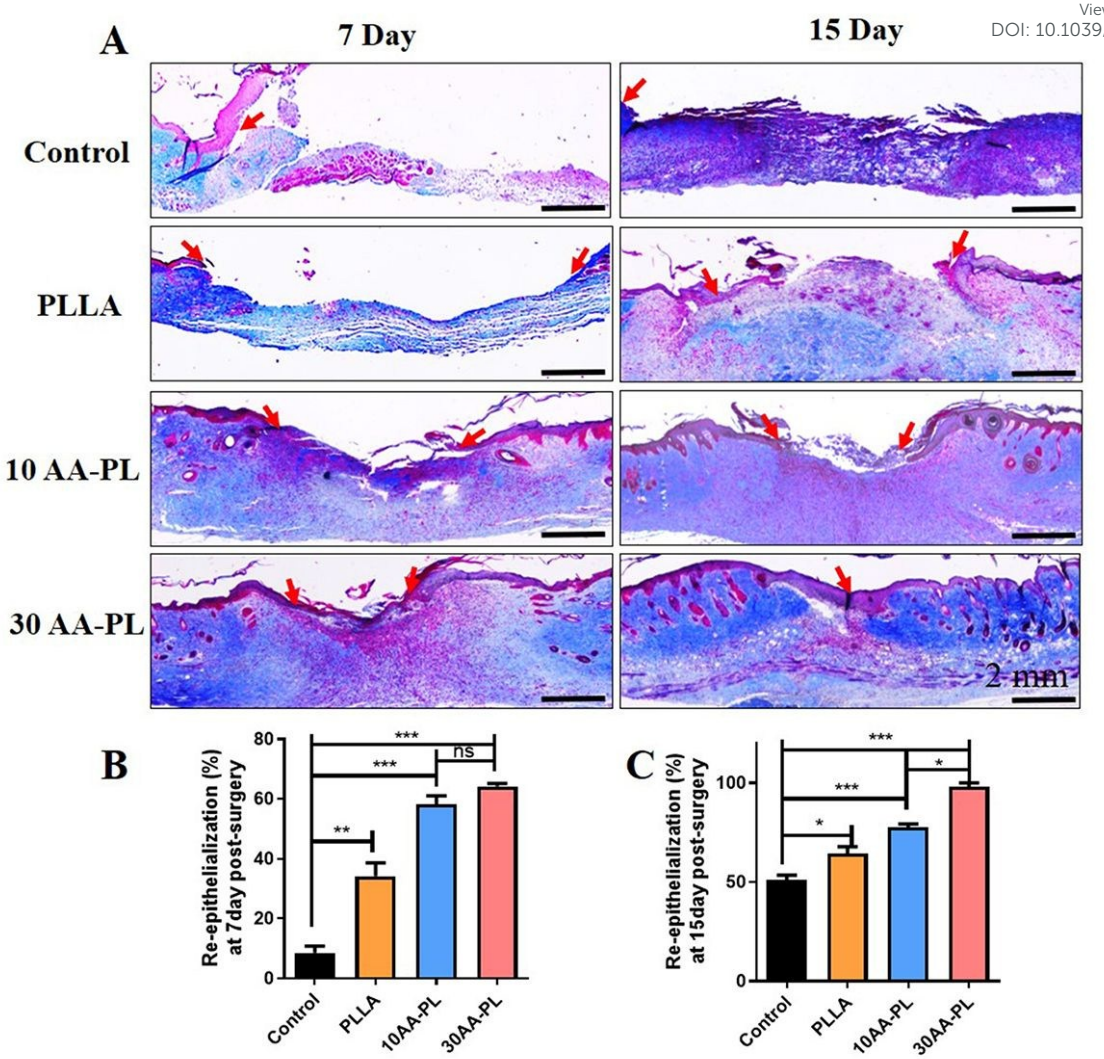

Figure 7. (A) Masson trichrome staining of the wounds tissues in the four groups (Ctrl, PLLA, 10 AA-PL and 30 AA-PL) at day 7 and day 15 after surgery (the edge of epithelium was pointed by the red arrows; scale bar = 2 mm). (B-C) Statistical analysis of re-epithelialization efficiency in different treated groups at day 7 (B) and day 15 (C) after operation. (* P< 0.05; **P < 0.01; *** P < 0.001)

View Article Online
DOI: 10.1039/C9TB01327J

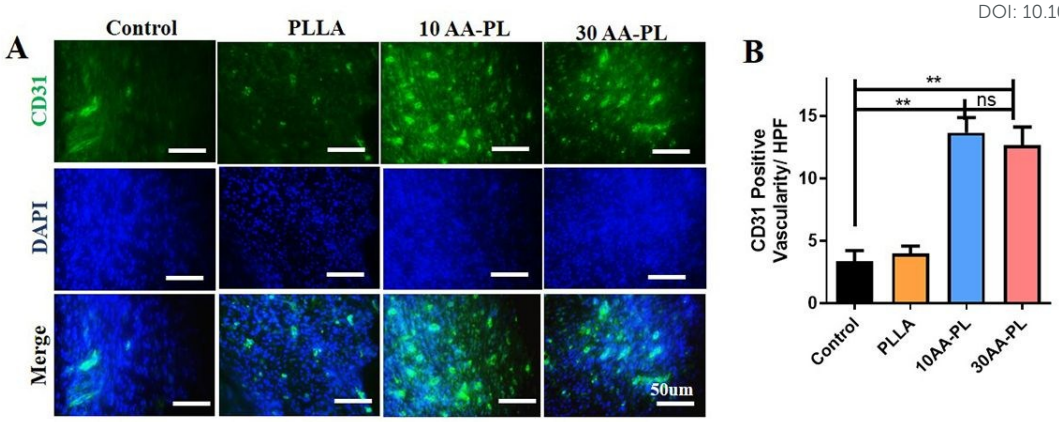

Figure 8. (A) CD31 immunofluorescence staining of the wounds tissue in different groups at 7 days after surgery, CD31 positive cells (Green, marked with red arrow) represents angiogenesis, cell nucleus (Blue) (scale bar = 50 μm); (B) Quantification analysis of CD31-positive vessels per high-power field (HPF) at day 7. (* P < 0.05; **P < 0.01; *** P< 0.001)

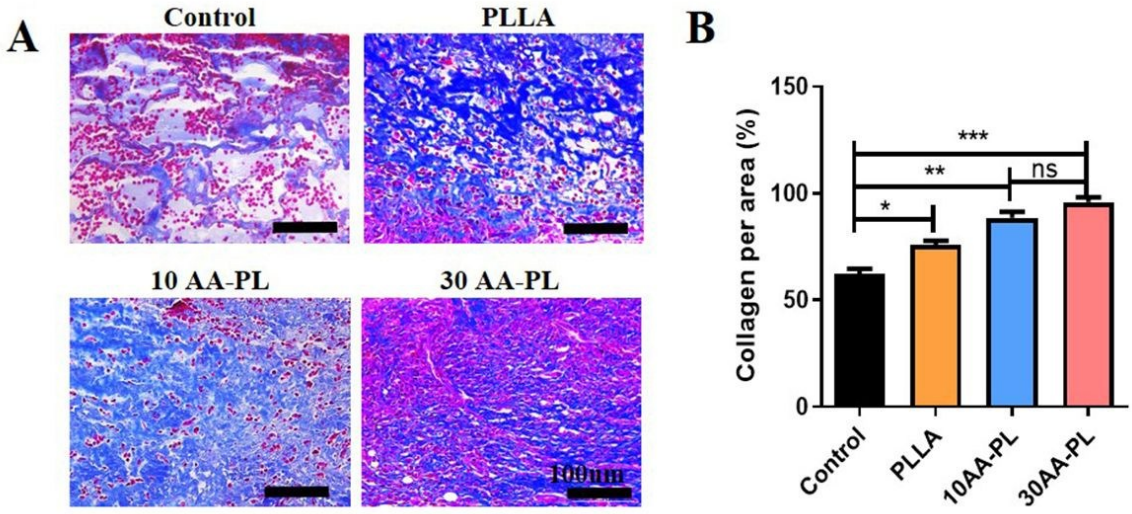

Figure 9. (A) Masson's trichrome staining of collagen fibers (blue) in the wound sites in the different groups (Ctrl, PLLA, 10 AA-PL and 30 AA-PL) at 15 days post-surgery (scale bar = 100 μm). (B) Quantification of the collagen-positive pixels per high-power field at day 15. （* P < 0.05; **P < 0.01; *** P< 0.001）

View Article Online
DOI: 10.1039/C9TB01327J

Table

Table 1. Primer Sequence List

Gene	Primer sequences
Actin-F	5-GTACGCCAACACAGTGCTG-3’
Actin-R	5’-CGTCATACTCCTGCTTGCTG-3’
IL-1β-F	5’-GCAACTGTTCCTGAACTCAACT-3’
IL-1β-R	5’-ATCTTTTGGGGTCCGTCAACT-3’
IL-6-F	5’-TAGTCCTTCCTACCCCAATTTCC-3’
IL-6-R	5’-TTGGTCCTTAGCCACTCCTTC-3’
TNF-α-F	5’-TTCCGAATTCAGTGGAGCCTCGAA-3’
TNF-α-R	5’-TGCACCTCAGGGAAGAATCTGGAA-3’

View Article Online
DOI: 10.1039/C9TB01327J